Chapter 1
Introduction

1.1 A Brief Historical Overview

Technological advances in many industries depend on the successful performance of parts produced by sintering of powders. More demanding applications of the sintered parts dictate new property requirements, which can be fulfilled only with the use of more efficient sintering techniques. Sintering is a process of consolidating powder particles into a bulk solid, which, in order to proceed, requires thermal activation of diffusion or other mechanisms of mass transport [1]. In traditional thermomechanical methods of powder processing, heat and pressure are the only tools to change the state of a material, and, thus, the possibilities of the conventional powder consolidation methods are limited in influencing the processes occurring in the powder compact during sintering.

Flexibility can be added to the sintering process by the introduction of electric and magnetic fields as sintering tools. A search for heating methods other than conventional furnace heating was stimulated by the need of higher-productivity processes and more uniform heating. Heat transport in initially porous bodies becomes a serious issue as the size of the part to be sintered increases. For conducting materials, a seemingly easy and convenient solution is volume heating by electric current. At present, the field-assisted powder consolidation methods present a matter of great scientific and practical interest, which is indicated by an enormous research activity in this area. The main reasons the field-assisted sintering methods have become so popular in the materials science community are the possibilities of sintering of a wide range of materials to high relative densities in a short time, at temperatures lower that in conventional sintering methods and with a control over grain growth.

Electric current was initially introduced in the field of sintering as a means of rapid heating. Heating filaments of the incandescent lights were introduced by Thomas Edison in the end of the 1870s [2]. The filaments were naturally consolidated during the initial stage of the electric current passage. This idea, however, while inherently present, was not explicitly formulated at that time. The author of the

E. A. Olevsky, D. V. Dudina, *Field-Assisted Sintering*,
https://doi.org/10.1007/978-3-319-76032-2_1

first patent on the application of resistance sintering is W. L. Voelker, who used a DC current to conduct his experiments on the consolidation of filaments of electric light bulbs in 1898 [3]. Resistance sintering was further developed by Sauerwald [4], who conducted the processes under pressure; Taylor [5], whose work had a goal to sinter refractory metals; and Lenel [6]. Soon it was realized that it is not only the presence or absence of current but also its application mode that have to be given particular attention. In the 1960s, patents by Inoue [7, 8] introduced electric discharge sintering, which served as a basis for the development of the spark plasma sintering (SPS) method and equipment by a Japanese company – Sumitomo Coal Mining Ltd. – in the 1990s. Impulse resistance sintering was used by Greenspan [9]. In that process, sintering started at a low pressure to benefit from heating of the contacts between the particles in the beginning of the process; the pressure was further increased as the sintering progressed. Also, microwave sintering and sintering by high-voltage electric pulses have been studied and developed independently for more than half-century, as described in the respective chapters of this book.

A number of review articles have been published since 1993 discussing the advantages and development strategies of field-assisted sintering techniques [10–22]. In these reviews, low-voltage pulsed current-assisted sintering, including SPS, has received particular attention [10–19]. The only monographs on field-assisted sintering are those written by Raichenko [23] and Belyavin et al. [24] published in Russian in 1987 and 1993, respectively. In electric current-assisted sintering, Belyavin et al. [24] saw a solution to the sintering challenges of refractory metals – a solution more promising than the introduction of low-melting-temperature additives. Although the monograph by Raichenko has been cited in research papers a great number of times, it has never been translated into English and remains accessible only to a limited audience. Many years have passed from the publication of this monograph; in these years, the field-assisted sintering has been greatly developed and strengthened by both research results and equipment design. A textbook on the methods of compaction and consolidation of nanostructured materials and products was published in 2008 by Khasanov et al. [25] in Russian, and only one chapter in it was devoted to field-assisted consolidation, namely, SPS.

Multiple possibilities of field application to powder and pre-compacted specimens make field-assisted sintering quite a broad area of solid-state research. This book is an attempt to summarize and critically analyze the up-to-date knowledge on the mechanisms of field-assisted sintering processes operating in different field application schemes. We did not aim at reviewing all successful sintering experiments and trials; many of them have been given credit in published reviews [17, 18]. In order to give the reader an understanding of what drives the sintering process when electromagnetic field is applied to the powder compact, we first briefly describe the phenomena that may be involved in the field-assisted sintering processes. In the following chapters, the physical principles and related equipment of high-voltage consolidation, low-voltage consolidation, flash sintering, induction heating sintering, microwave sintering, magnetic pulse compaction, and some other field-assisted sintering techniques are presented along with the analysis of

the relevant theoretical and experimental work elucidating the process mechanisms. At the end of each chapter, selected examples of materials produced by field-assisted sintering are given to show the potential of those sintering methods for practical applications.

The concept of field-assisted sintering allows a wide range of field and pressure application schemes. According to the classification presented by Grasso et al. [18], the processes of pulse electric current-assisted powder sintering can be divided into fast techniques (the current is applied for durations longer than 0.1 s) and ultrafast techniques (the current is applied for durations shorter than 0.1 s). Fast processes are characterized by durations of up to several minutes, current densities reaching 1 kA cm^{-2} and voltages of several volts. The powder sintering facilities using this mode of electric current application include a standard electric pulse generator providing low voltages and high electric currents to the sample. The duration of each pulse ranges from 1 to 300 ms. The pulses are applied to the sample for a total duration of several minutes or tens of minutes. The fast methods are suitable for sintering of both conductive and non-conductive materials. The ultrafast methods usually require relatively high applied pressures (up to several GPa) and very high current densities ($\geq$10 kA cm^{-2}). The voltages vary from several volts to several kilovolts. The discharges with durations of 10^{-5}–10^{-1} s are generated by capacitors. The ultrafast methods are mostly suitable for conductive materials[1].

In the area of sintering assisted by pulsed current, several terms are used to refer to one and the same sintering method. This situation developed as scientists and equipment engineers tried to emphasize different aspects of the developed methods. The same method and equipment can be referred to using different terms in publications by different authors, while one and the same term is often used to refer to methods principally different from each other by the current application scheme. Additional variations of the terms denoting field-assisted sintering techniques appear when those are translated into English from another language.

Belyavin et al. [24] suggested a classification of the field-assisted sintering methods, in which they are grouped by the character of the physical processes involved in heating of the powder material (Fig. 1.1). Direct heating of the powder occurs whenever a current passes through the compact. Indirect heating can be caused by several phenomena associated with electric current. None of the indirect heating methods can be considered versatile, each being suitable for selected applications. The main advantages of induction heating are high heating rates and a possibility of concentrating a high power in a small volume of the material. However, the physical and chemical processes involved in induction heating-based sintering are still rather poorly understood on a microscopic level.

The characteristic values of the parameters of field-assisted sintering techniques are presented in Table 1.1. The following terms are used to refer to high-voltage (mostly ultrafast) processes of sintering that employ electric current applied in a pulsed mode: electric pulse pressing (EPP), electric discharge sintering (EDS),

[1]Material's electric and thermal conductivities may rapidly change during heating.

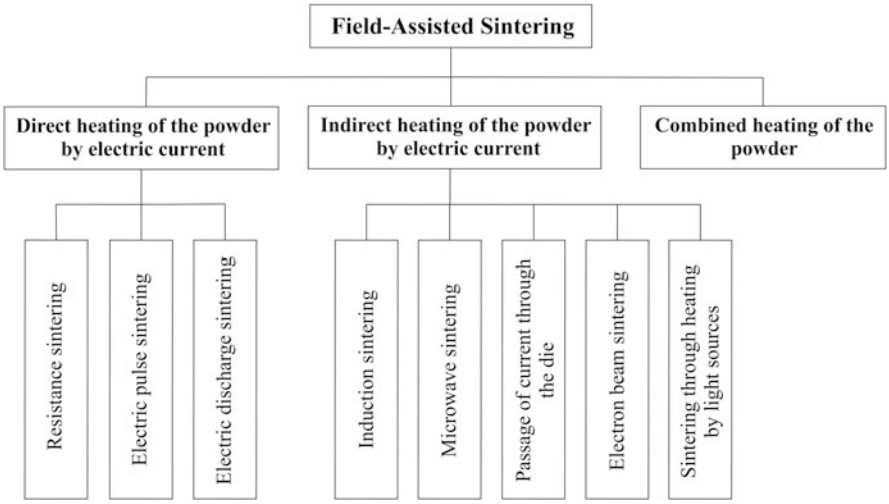

Fig. 1.1 Classification of the field-assisted sintering methods by the heating method of the powder materials. (Drawn using data of Ref. [24])

Table 1.1 Characteristic values of the parameters of field-assisted sintering methods

Field-assisted sintering method	Field application mode	Total process duration	Pressure
Resistance sintering	DC, AC currents	10^{-2}–10^{2} s	10 MPa-1 GPa
High-voltage electric discharge consolidation	Current pulse from a capacitor discharge	<1 s	10 MPa-1 GPa
Flash sintering	DC current	Several seconds	No pressure
Electric discharge sintering, spark plasma sintering (SPS)	Pulsed DC	1–20 min	10 MPa-1 GPa
Sintering in the constant electric field in the noncontact mode	Low DC current or no current through the sample	Several minutes	No pressure
Microwave sintering	Microwave radiation	Several minutes	No pressure
Induction heating sintering	AC	1–20 min	10 MPa-1 GPa
Magnetic pulse compaction (MPC)	Acceleration of the impactor by magnetic field generated by a current pulse from a capacitor discharge	<1 s	Several GPa

electric discharge compaction (EDC), pulsed electric discharge (PED), high-rate electric discharge compaction (HREDC), environmental electric discharge sintering (EEDS), capacitor discharge sintering (CDS), pulse plasma sintering (PPS), and electric pulse sintering (EPS). Low-voltage consolidation is usually referred to as

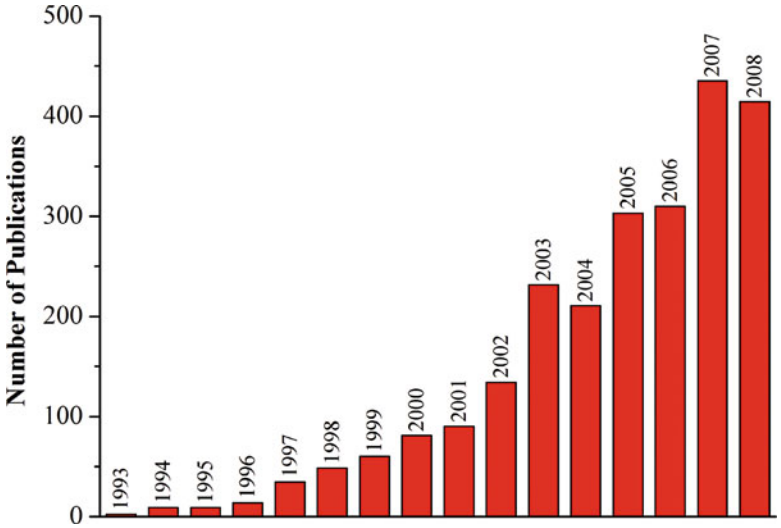

Fig. 1.2 Statistics of publications on spark plasma sintering. (Reprinted from Munir et al. [16], Copyright (2010) with permission of John Wiley & Sons)

Fig. 1.3 Statistics of publications and patents on spark plasma sintering

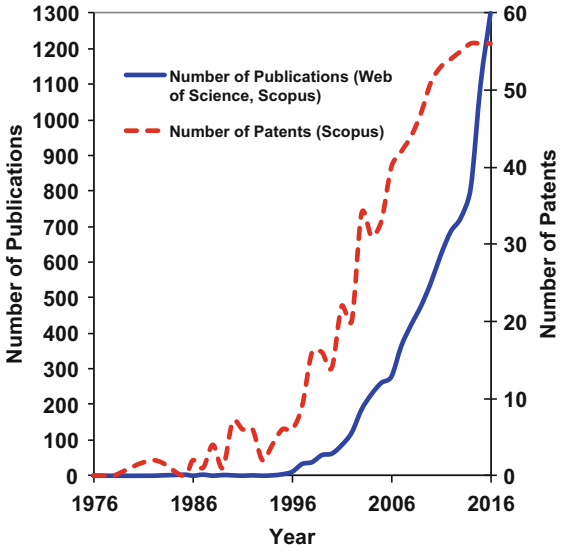

spark plasma sintering (SPS), electric discharge sintering (EDS, especially in the literature published in Russian [23]), pulsed electric current sintering (PECS), or field-assisted sintering technique (FAST). The statistics of publications on SPS from 1993 to 2008 is presented in Fig. 1.2 [16]. The statistics of publications and patents on SPS from 1973 to 2006 was provided in Ref. [26] and extended in Fig. 1.3 to

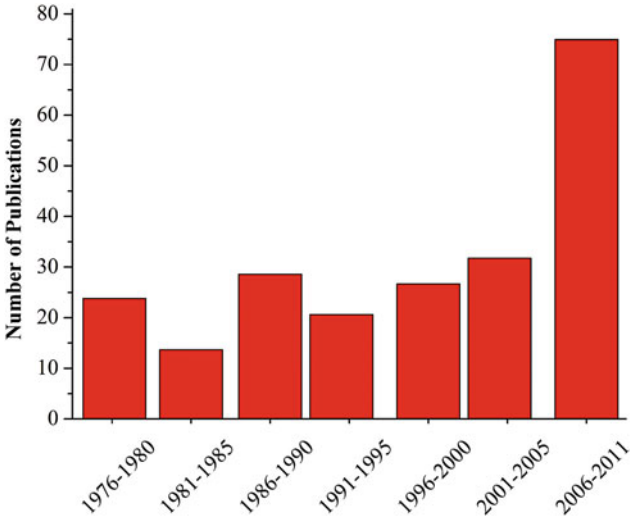

Fig. 1.4 The number of publications on electric pulse sintering (high-voltage techniques). (Reprinted from Yurlova et al. [22], Copyright (2013) with permission of Springer)

2016. The number of publications on electric pulse sintering (high-voltage techniques) over the 1976–2011 period is shown in Fig. 1.4 [22].

Electric discharge sintering (EDS, a low-voltage technique) should, in a general case, include two different stages, the first one favoring the formation of discharges between the particles for efficient heating of the contacts, and the second one favoring densification [23, 27]. Some authors use the term "electric discharge sintering" to refer to a two-stage process, the first stage of which is a high-voltage pulse, while the second stage includes the action of an electric current of high density and lasts several tens of minutes [28]. During the first stage, even in powders having an oxide film on the particle surface, the inter-particle contacts successfully form, promoting efficient sintering at the second stage.

1.2 Thermal and Nonthermal Effects in Field-Assisted Sintering

Most of the studies conducted on field-assisted sintering are based on experimental trial-and-error attempts to consolidate various powder systems. One of the most important questions is which factors provide accelerated densification and, in many cases, limited grain growth in field-assisted sintering compared with regular hot pressing applied to the same material systems. The difference between the outcomes of field-assisted and conventional powder hot consolidation processes can be attributed to various physical factors, which are grouped as phenomena of thermal nature and those of nonthermal nature corresponding to the so-called field effect.

1.2.1 Thermal Effects in Field-Assisted Sintering

The group of factors of thermal nature may include [26]:

1. High heating rates, which enable higher sinterability of the powders
2. High local temperature gradients, which provide conditions for thermal diffusion
3. Highly nonuniform local temperature distributions, which cause local melting within inter-particle contact areas
4. Highly nonuniform macroscopic temperature distributions, which create thermal stresses intensifying dislocation creep

It has been shown that high heating rates increase the sinterability of powder compacts by suppressing surface diffusion at the early stages of sintering. High heating rates also ensure limited grain growth. Experimentally, it has been shown in a number of investigations that an increase in the heating rate considerably increases the consolidation rate of conductive and non-conductive powders during SPS. For an alumina powder, it was shown that switching from a heating rate of 50 °C·min^{-1} to a heating rate of 300 °C·min^{-1} while keeping the same maximum temperature allowed decreasing the sintering time by a factor of six and reaching the same final density [29]. Physically, this was explained by the presence of additional defects in the material directly related to high heating rates and a short duration of the process. Johnson [30] qualitatively showed that high heating rates minimize the effects of surface diffusion processes not contributing to densification; hence, the compact body reaches higher temperatures in a highly sinterable state. From the modeling studies conducted by Olevsky et al. [26] for the SPS process, it was concluded that surface diffusion contributes to the evolution of the pore surface curvature, thereby influencing the intensity of grain-boundary diffusion at the early stages of sintering. The interaction of surface and grain-boundary diffusion is thus one of the major mechanisms enabling the impact of heating rates on the consolidation kinetics. Another heating rate-sensitive contribution to the densification is related to the shrinkage kinetics by power-law creep accelerated by a rapid increase in temperature. Both the calculations and the experiments [26] show an increase in the maximum shrinkage rate for larger particle sizes. This mostly unusual for conventional powder sintering and hot pressing phenomenon is explained under conditions of rapid heating by the delayed pore tip spheroidization and the intensification of grain-boundary diffusion at early stages of sintering for larger grain sizes.

In contrast to conventional powder consolidation techniques, high local temperature gradients caused by nonuniform current distribution in the compacts at the scale of the particle size can instigate additional driving forces for consolidation. Ludwig–Soret effect of thermal diffusion leads to the formation of concentration gradients in initially homogeneous two-component systems subjected to a temperature gradient [31]. For the case of atomic and vacancy diffusion in crystalline solids, this effect was studied by a number of authors; its theoretical interpretation was conducted by Shewmon [32] and Schottky [33]. For the electric current-assisted sintering, the effect of thermal diffusion was analyzed by Kornyushin [34]. Later, for

rapid densification, the role of temperature gradients was studied by Searcy [35] and Young and McPherson [36]. Johnson [30], however, argued against the significance of thermal diffusion for the sintering enhancement in microwave sintering in a debate with Young and McPherson [37].

On a microscopic scale, the electric field lines become denser when the current flows around the pores, which leads to a local temperature rise and the formation of large temperature gradients. Gostomelskiy and Krupnova theoretically analyzed the growth and healing processes of isolated pores in a metal subjected to pulses of electric current [38]. They concluded that heating of the metal by electric pulses intensifies the healing (disappearance) of pores in comparison with furnace heating up to the same final temperatures. As the temperature of the pore surface is higher than the volume temperature, the temperature gradient leads to the diffusion of vacancies in the pores resulting in the pore growth. At the same time, the vacancy concentration gradients form due to rapid heating. While a certain time is needed for the vacancy concentration to reach its equilibrium value corresponding to the temperature in the volume of the material, this occurs instantaneously at the pore surface. Consequently, the vacancies diffuse from the vicinity of large pores resulting in the pore healing. To reduce the temperature gradients, the sintering process should consist of short multiple pulses (10^{-5} s) with an interval between them one or two orders of magnitude longer than the duration of the pulse. Large pores are reduced in size at a higher rate, which is related to the vacancy flux being proportional to the surface area of a pore. The reduction of porosity will be successfully achieved if the heating of the material by electric pulses is such that the temperature gradients due to the presence of pores potentially leading to the pore growth are not high, while the vacancy gradients between the pore surface and the volume of the material are sufficient to heal the pores. The healing of large pores can be looked upon as the reaction of the system to the increased intensity of the electric field in the vicinity of pores as the diffusion of vacancies from the regions surrounding large pores in the direction of smaller ones reduces the differences in the intensity of the electric field.

A possible contribution of thermal diffusion to the SPS processes has been discussed by Olevsky and Froyen based on modeling results presented in Ref. [39]. The calculation results indicated that local temperature gradients (concentrated in the area of inter-particle contacts) can exceed the macroscopic temperature gradients by 3–4 orders of magnitude. The intensity of thermal diffusion increases for higher pulse frequencies. Thermal diffusion promotes the separation of atoms and vacancies. At the early stages of sintering, this should lead to the growth of inter-particle necks, which corresponds to the enhancement of sintering. At the final stages of sintering, however, the pores may serve as vacancy sinks under thermal diffusion conditions, which impedes sintering. It is possible that the increased pulse frequencies enhance sintering at the early stages of SPS and hinder sintering at the late stages. In some experimental studies, the pulse frequency was found to have a limited impact on the SPS results [40]; its contributions at early and late stages of SPS could have offset each other.

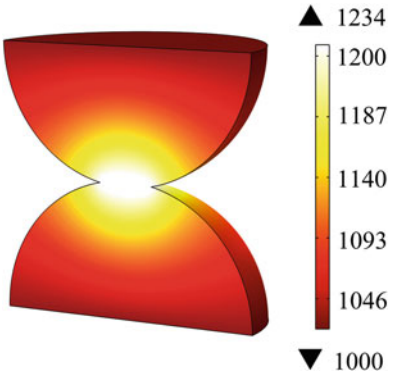

Fig. 1.5 Temperature distribution obtained by modeling of the resistance heating of spherical copper particles 10 μm in diameter

Resistance heating of two spherical particles was modeled by Kuz'mov et al. [41] for spherical particles having a thin oxide film on their surface. In practice, the presence of oxide films on the surface of metallic powders is rather common. The model allowed obtaining the dependences of the temperatures and the temperature gradients on the contact voltage and the relative contact resistance. The contact voltage is the potential difference between the centers of the particles. In the calculations, it was varied from 0.01 V to 0.4 V. The relative contact resistivity k_ρ was calculated as follows:

$$k_\rho = \frac{h}{r} \cdot \frac{\sigma_0}{\sigma}, \tag{1.1}$$

where h is the thickness of the oxide film, r is the particle radius, σ_0 is the electrical conductivity of the material of the particle, and σ is the electrical conductivity of the oxide film. As can be seen in Fig. 1.5 showing the temperature distribution obtained by modeling of the resistance heating of spherical copper particles 10 μm in diameter, the temperature of the inter-particle contacts is substantially different from the average macroscopic temperature of the sample. Figure 1.6 shows the parametric isolines of the average temperature. Unlike temperature, its gradient is inversely proportional to the particle size. If the contact resistivity is constant, the temperature gradient increases with decreasing particle size. The temperature gradients in the contact region between the powder particles with a size of 10 μm exceed 10^6 K·m^{-1}. Such temperature gradients may have a noticeable effect on mass transfer by the mechanisms of thermal diffusion and non-equilibrium distribution of vacancies [36]. If the particle size is varied, while the voltage drop across a macroscopic sample (i.e., macroscopic electric field strength) is kept constant, the contact voltage is proportional to the size of the contacting particles, and the gradient decreases with this size. This is because the inversely proportional relationship between the temperature gradient and the particle size cannot balance the nonlinear (nearly parabolic) dependence on contact voltage. The maximum temperature gradient (Fig. 1.7) differs from the average gradient in that it does not tend to zero as the

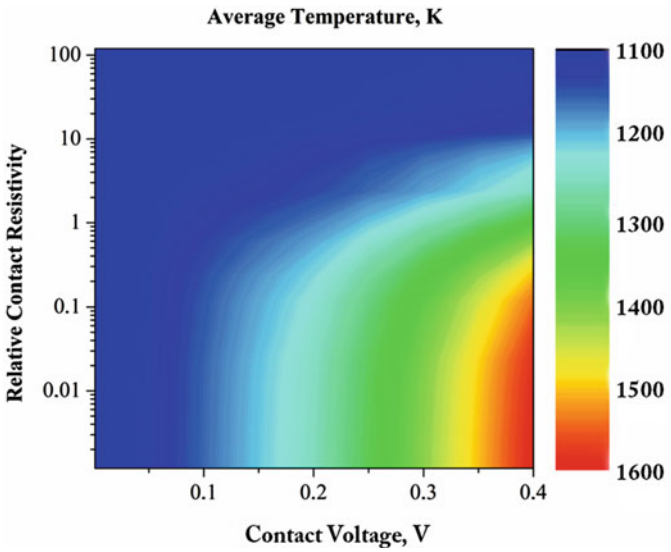

Fig. 1.6 Parametric isolines of the average temperature obtained using modeling of the resistance heating of spherical copper particles 10 μm in diameter. (Drawn using data of Ref. [41])

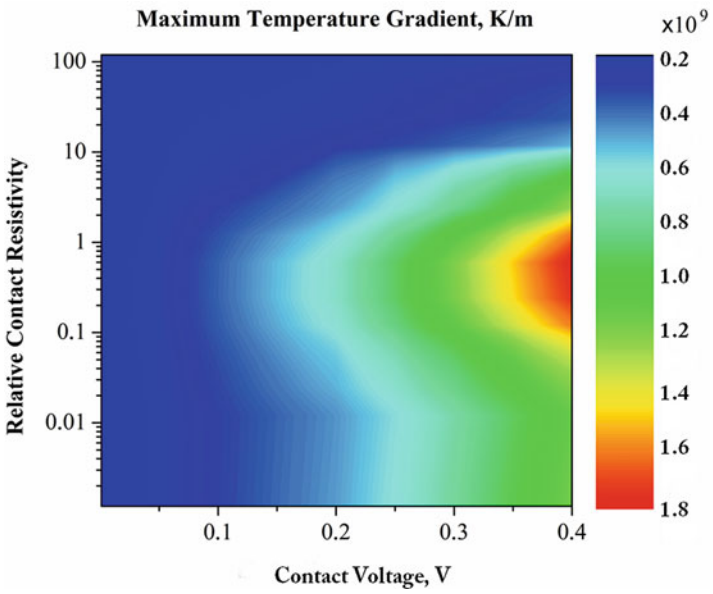

Fig. 1.7 Parametric isolines of the maximum temperature gradient obtained using modeling of the resistance heating of spherical copper particles 10 μm in diameter. (Drawn using data of Ref. [41])

contact resistivity tends to zero. In other respects, the behavior of these quantities is similar, and the above reasoning on the average gradient is true for the maximum gradient. It was shown [36] that the resistance heating of a powder can cause melting in the contact region at very low macroscopic temperature.

The fact that the local temperature at the inter-particle contact region may be much higher than the macroscopic temperature of a consolidating body should be taken into account when shrinkage of the powder compact is described. Since the neck between the particles is also a region of major deformation, especially at the early stages of consolidation, resistance heating causes faster shrinkage than conventional furnace heating at the same temperature and external pressure. The power-law creep equation [42] can be used to prove that even a difference of a few hundred degrees in the temperature causes a significant increase in the shrinkage rate of the powder compact:

$$\dot{\gamma} = A\frac{D_{\mathrm{v}}Gb}{kT}\left(\frac{\sigma_s}{G}\right)^n, \quad D_{\mathrm{v}} = D_{\mathrm{v}0}\exp\left(-\frac{Q_{\mathrm{v}}}{RT}\right) \tag{1.2}$$

In Eq. (1.2) $\dot{\gamma}$ is the shear strain rate, A is a dimensionless constant, D_{v} is the lattice diffusion coefficient, G is the shear modulus, b is the Burgers vector, σ_s is the shear stress intensity, and Q_{v} is the activation energy of diffusion.

While the local temperature gradients lead to thermal diffusion of vacancies, the macroscopic temperature gradients lead to thermal stresses. The thermal stresses, being internal stresses for a porous specimen, cannot independently contribute to the overall macroscopic volume shrinkage. They, however, can impact the processes of the generation and motion of dislocations, which can influence the diffusion rates during sintering. Tuchinskii [43, 44] analyzed thermal stresses in porous compacts originated from a nonisothermal state of the specimen at the beginning of heating. A situation, in which a porous cylinder is heated from its external surface placed in an atmosphere of a constant temperature exceeding that of the initial temperature of the cylinder, was considered. By analyzing the equations for the radial σ_r and peripheral stress σ_θ over the cross section of the cylinder, it was found that the peripheral stress is greater in absolute magnitude than the radial stress. On the cylinder axis, the stresses are equal to each other: $\sigma_r = \sigma_\theta$. During heating of the specimen, the radial stress is tensile throughout the volume of the cylinder increasing from zero on the specimen surface to $\sigma_r = \sigma_\theta$ on the cylinder axis. The peripheral stress in the outer layers is compressive. It reaches its maximum absolute value on the cylinder surface and then decreases reaching zero at a certain distance from the cylinder axis. After that, it changes sign becoming tensile and grows in magnitude.

Tuchinskii emphasizes that thermal stresses alone acting inside the porous body cannot lead to volume shrinkage of the compact as the hydrostatic pressure generated by the thermal stresses averaged throughout the volume is equal to zero. A possible mechanism of activation of sintering under nonisothermal conditions may be related to the generation and motion of dislocations under the action of thermal stresses, which, in turn, accelerate the diffusion processes responsible for mass transport. The thermal stresses can exceed the Laplacian stress. In order to conclude

on the ability of thermal stresses to make dislocation sources active, the rms values of thermal stresses, equations for which were derived in Ref. [45], should be compared with the yield stress of the material. Taking into account the dependence of the yield stress on the temperature in his calculations, Tuchinskii showed that thermal stresses generated during rapid heating of a porous nickel compact (at heating rates characteristic of induction heating) are high enough to cause plastic deformation in the outer and inner layers of the compact, actuate Frank–Read sources, and, thus, enhance sintering. In conventional furnace sintering, thermal stresses are likely to reach the value of the yield stress of the material only in the outer layers of the compact [43]. A critical heating rate parameter was introduced in Ref. [44] to conclude on the possibility of plastic relaxation of thermal stresses. At heating rates exceeding the critical value, the dislocation sources become operative, and generation of new dislocations can be expected in the material.

1.2.2 Nonthermal Effects in Field-Assisted Sintering

The nonthermal group of factors contributing to enhanced densification in field-assisted sintering may include [26]:

1. Electromigration and intensified diffusion in ionic conductors
2. Electroplasticity effects
3. Ponderomotive forces
4. Electromagnetic "pinch" effect
5. Dielectric breakdown of oxide films (cleansing effect) and defect generation at grain boundaries
6. Plasma formation

Nonthermal effects of electric current were studied experimentally by Asoka-Kumar et al. [46] and Garay et al. [47]. They used positron annihilation spectroscopy to obtain information on the defect concentrations in solid materials subjected to electric current. Asoka-Kumar et al. showed that an electric current of a density of $8 \cdot 10^4$ A·cm^{-2} passing through the Al-0.5 wt.%Cu alloy induces the dynamic formation of vacancies. The increase in the vacancy concentration was substantially greater than that caused by thermal generation alone (4×10^{18} cm^{-3} vs. 3×10^{17} cm^{-3}). Garay et al. found that a DC current increases the kinetics of annealing of the previously stored defects in Ni_3Ti and attributed the observed effect to the electron wind, although no dependence of the effect on the direction of electric current was observed. A lack of asymmetry could be a consequence of the complex crystalline structure of the Ni_3Ti intermetallic, in which the diffusion of one element is coupled with diffusion of the other because the structure and stoichiometry have to be maintained. These results shed light on the mechanism of the influence of electric current on solid-state chemical reactions involving metals.

Frei et al. [48] showed that DC current has a marked effect on neck growth between copper spheres 3 mm in diameter and copper plates using a SPS apparatus

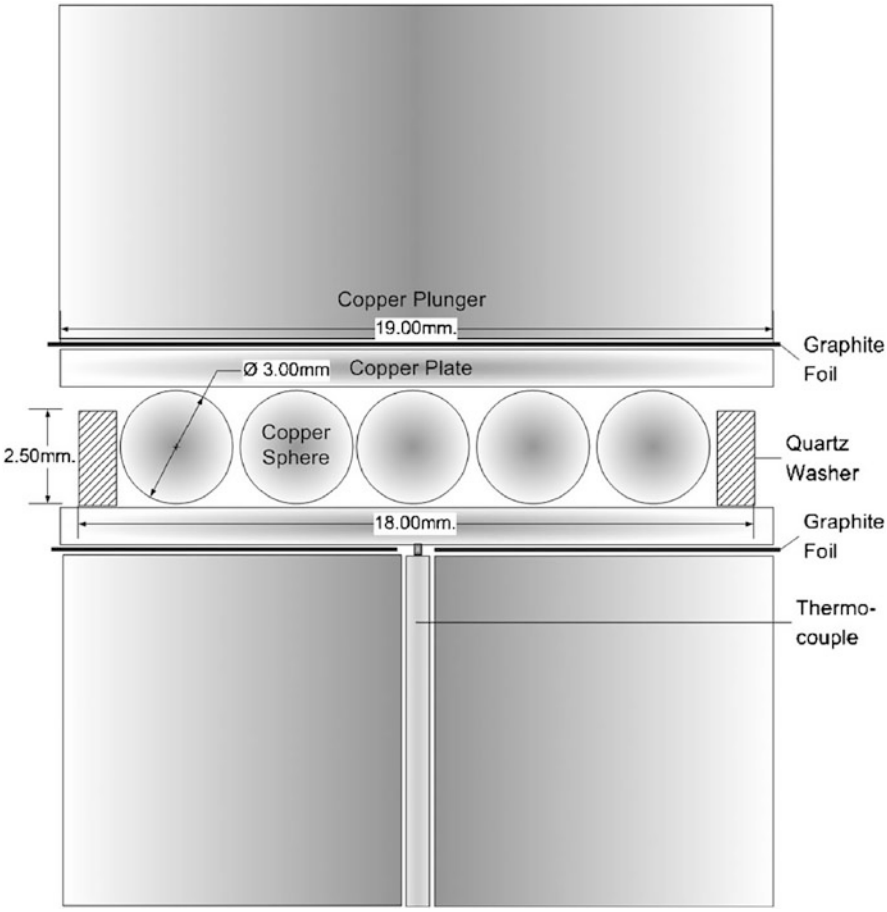

Fig. 1.8 Schematic of the experiment with copper spheres between copper plates to study the effect of current on neck growth in a pulsed electric current sintering apparatus. (Reprinted from Frei et al. [48], Copyright (2007) with permission of AIP Publishing)

and a modified die/punch assembly that allowed separating the influence of the temperature and the current (Fig. 1.8). In a general case of current-assisted sintering, the current and the temperature of the compact are dependent parameters. Since the only source of heat is Joule heating, the power generated to maintain a steady-state temperature is constant. By introducing a stack of alternating copper disks and graphite foils into the SPS die assembly, it was possible to vary the current passing through the sample at a constant electric power (and, consequently, at a sample constant temperature). The resistance of the graphite foil and the contact resistance in this case made the dominant contribution to the resistance of the assembly. The effect of current on neck growth is seen in Fig. 1.9 showing images of the areas on the lower copper plate that were sinter-bonded to copper spheres after their separation.

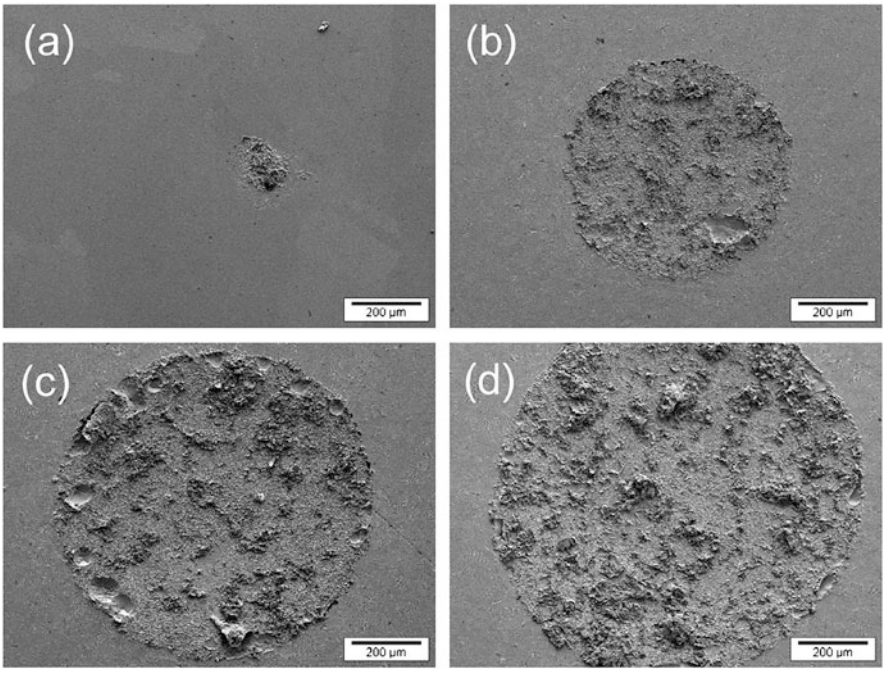

Fig. 1.9 Scanning electron microscopy images of the areas on the lower copper plate that were sinter-bonded to copper spheres at 900 °C for 60 min: (**a**) no current, (**b**) 700 A, (**c**) 850 A, (**d**) 1040 A. (Reprinted from Frei et al. [48], Copyright (2007) with permission of AIP Publishing)

The experimental data were fitted into the equation for the initial stage of sintering for a simplified model of spherical particles sintered at a constant temperature

$$\left(\frac{x}{R}\right)^n = \frac{Bt}{R^m}, \tag{1.3}$$

where B is a constant containing the diffusion coefficient, R is the radius of the sphere, x is the diameter of the neck, t is the time, and n and m are sintering mechanism-dependent constants. Values of sintering exponent n that were found showed that no classic sintering mechanism could be applied to describe the process. An interesting observation was the formation of voids in the neck region, especially at the edge region (Fig. 1.10). The size of the voids increased with the sintering time.

The correlation of sintering enhancement with the level of current demonstrated by Frei et al. [48] was explained by electromigration. The flux J_i of the diffusing species "i" is a result of the momentum transfer from the electron wind effect:

$$J_i = -\frac{D_i C_i}{RT}\left[\frac{RT\partial \ln C_i}{\partial x} + Fz^* E\right] \tag{1.4}$$

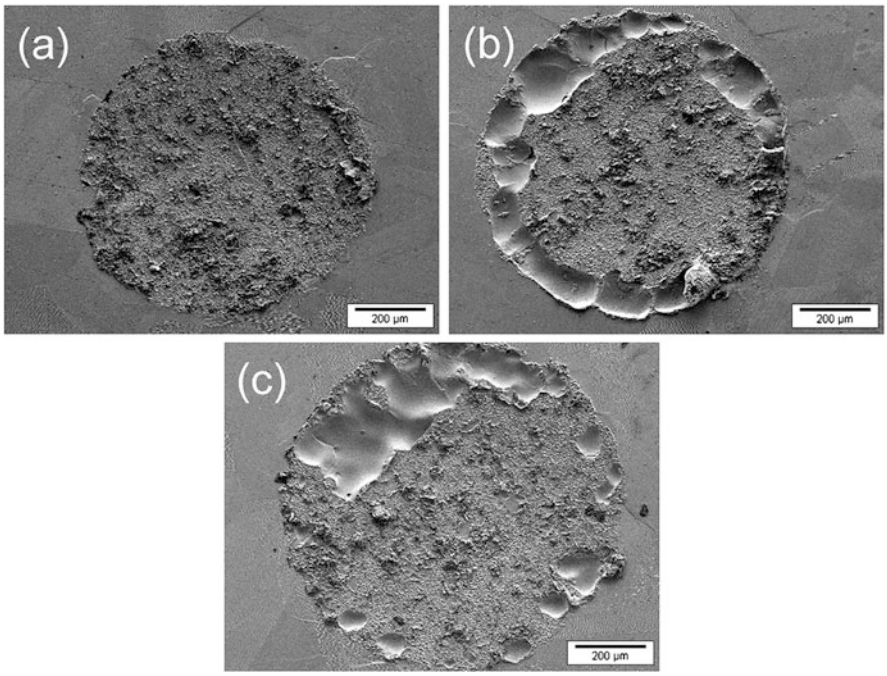

Fig. 1.10 Scanning electron microscopy images of the areas on the lower copper plate, which were sinter-bonded to copper spheres, total current 1040 A, temperature 900 °C: (**a**) 15 min, (**b**) 30 min, (**c**) 60 min. (Reprinted from Frei et al. [48], Copyright (2007) with permission of AIP Publishing)

D_i is the diffusivity of the ith species, C_i is the concentration of the species, F is Faraday's constant, z^* is the effective charge on the diffusing species, E is the field, R is the gas constant, and T is the temperature. A large size of the voids observed in these experiments raises a question of the scale of the electromigration-induced effects.

An interesting observation was the presence of ledges on the surface of the copper plate, which became less abundant as the distance from the neck increased. The occurrence of these ledges was related to the current, as they were not observed in experiments conducted in the absence of current. The formation of the ledges was attributed to the effect of surface electromigration on evaporation.

Burenkov et al. [49] provided evidence of the operation of mechanisms other than diffusion during electric current-assisted sintering of porous compacts. With diffusion mechanisms operating, the linear size of the neck between particles X depends on the sintering time t according to a power relationship $X^n \sim t$. For volume diffusion, $n = 5$, while for surface diffusion, $n = 7$. Although this relationship is valid for isothermal conditions, it was considered applicable for the estimation of the neck growth exponent in the electric current-assisted processes. The values of n were found to vary in a wide range – from 0.5 to 5. These estimates, especially the

observed cases of very low n, are of great importance for the understanding of the sintering mechanisms, as they point to the operation of very vigorous processes, such as viscous flow and spreading of the liquid metal squeezed out of the contact zone over the solid surfaces. There was no fundamental difference in the interaction between the contacting particles located along the line parallel to the direction of the current and between those located along the line perpendicular to the direction of the current.

The role of melting processes in establishing the inter-particle contacts was addressed by Belyavin et al. [24]. They observed experimentally and described mathematically the processes at inter-particle contacts, the main feature of which was local melting. The behavior of the molten column formed between the particles, namely, shape changes of the molten column, a stability loss, and squeezing of the molten metal from the contact area, depends on the relative influence of the applied mechanical pressure, electromagnetic forces, and surface tension. If mechanical pressure squeezes the molten metal from the inter-particle contact area, the size of the contact decreases and so does its mechanical strength.

A constitutive model of SPS taking into consideration the direct contribution of electric current to grain-boundary diffusion was developed by Olevsky and Froyen [50]. They constructed a densification map for an aluminum powder consisting of three porosity/grain size domains. In each of these domains, one of the three considered driving factors of material transport – externally applied load, surface tension, and electromigration – is dominant (Fig. 1.11). The power-law creep induced by an external stress always dominates for higher porosities. For lower porosity values, the electromigration can become the dominant mechanism, and for smaller particle sizes and low porosity, surface tension is the main driving factor for densification. For very small porosities in the electromigration-dominating zone, the ultimate collapse of voids may require externally applied load as the primary factor.

A significant contribution of high-intensity fields to the materials deformation can be expected thanks to electroplasticity effects [51]. During deformation of aluminum alloy Al7475 in a DC field (field intensity 2 $kV \cdot cm^{-1}$), the flow stress and the strain hardening exponent of the superplastic deformation were reduced by the electric field, while the strain rate sensitivity exponent was increased. The fracture surface of the specimen tested under the electric field showed the presence of whiskers, whose formation could not be explained by diffusion or dislocation-involving mechanisms because of very high degrees of deformation near the grain boundaries that must occur for such whiskers to form (Fig. 1.12). Therefore, viscous flow of a quasi-liquid was suggested as an explanation of the observed fracture morphology. The application of a DC field led to a number of effects, including dissolution and coalescence of the dispersoids in the alloy and formation of dispersoid-free zones near the grain boundaries.

A reduction in the flow stress during the tensile deformation of ceramics at high homologous temperatures was analyzed by Conrad and Yang for fields $<500\ V \cdot cm^{-1}$ [52]. The Joule heating was considered as giving only a minor contribution to the reduction of the flow stress. The main mechanism was a decrease

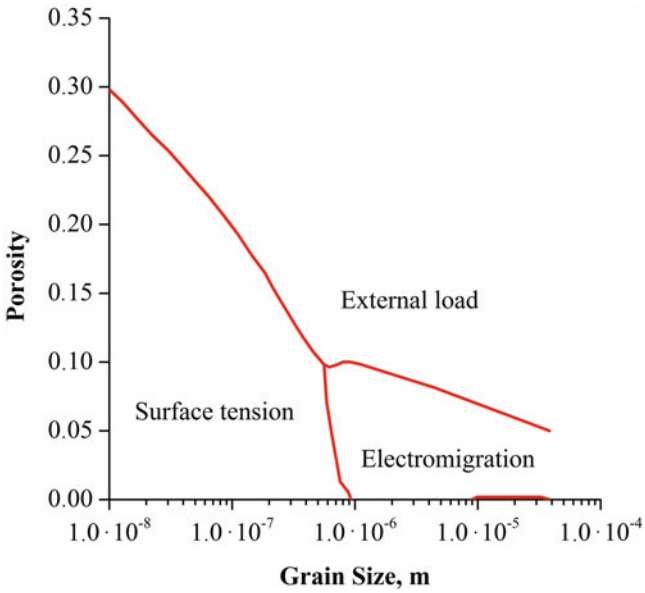

Fig. 1.11 Densification map for Al powder, $\frac{U}{l} = 417\ ^{V}/_{m}, T = 673\ K, \overline{\sigma}_x = 283$ MPa. (Reprinted from Olevsky and Froyen [50], Copyright (2006) with permission from Elsevier)

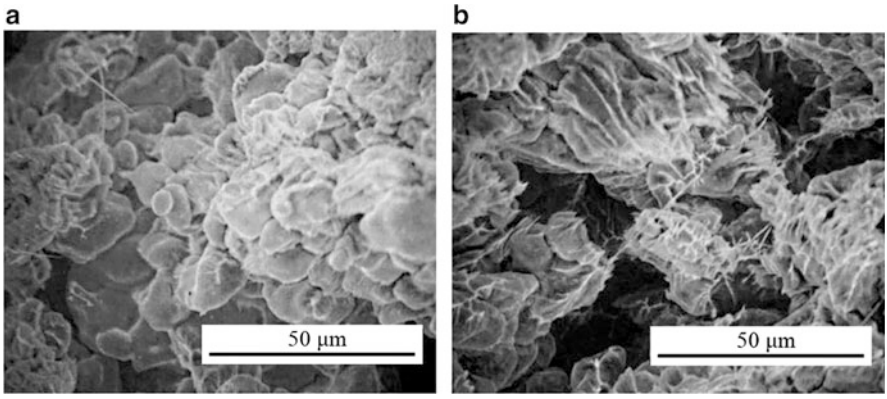

Fig. 1.12 Fracture surface of Al7475 tested without electric field (**a**) and at an applied field with an intensity of 2 kV/cm (**b**) at 516 °C. (Reprinted from Cao et al. [51], Copyright (1990) with permission from Elsevier)

in the potential of the vacancy formation corresponding to the diffusion of the rate-controlling ions in the space-charge region at grain boundaries. It was concluded that, for some oxides, dynamic grain growth is retarded by the electric field influencing grain-boundary mobility within the space-charge zone.

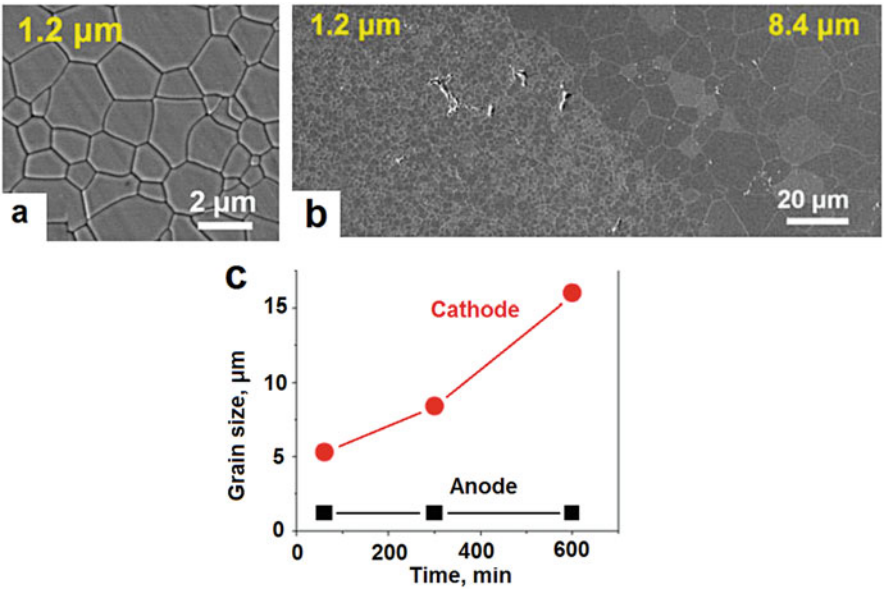

Fig. 1.13 Microstructure of the initial fully dense yttria-stabilized zirconia containing 8 mol.% of Y_2O_3 obtained by hot isostatic pressing, average grain size 1.2 μm (**a**), region of step transition of the grain size in the sample subjected to a current density of 50 A ·cm^{-2} for 300 min at 1340 °C (**b**) and grain size evolution at the anode and cathode sides of the sample with time at 1350 °C and a current density of 50 A ·cm^{-2} (**c**). (Reprinted from Kim et al. [53], Copyright (2011) with permission of John Wiley & Sons)

Kim et al. [53] reported the influence of DC currents on the grain growth of yttria-stabilized zirconia (Fig. 1.13). In their experiments, pre-sintered specimens of yttria-stabilized zirconia were annealed in a furnace with and without the application of a DC current. The microstructure of the fully dense pre-sintered specimen is shown in Fig. 1.13a. The sample temperature was higher than the set furnace temperature due to Joule heating when the current density was greater than 20 A·cm^{-2}. Grain growth in the electrically loaded samples depended on the location. Enhanced grain growth was observed at the cathode side of the specimen (Fig. 1.13b, c). In a fully dense sample subjected to a DC current, the grain growth started at 1150 °C at the cathode side, which is well below the conventional sintering temperature. The lower limit for the current density to trigger grain growth at 1150 °C was 1.5 A·cm^{-2} (from 1.2 to 1.5 μm after 24 h of annealing). Without an electric current, there were no grain growth at 1250 °C and only a slight increase in the grain size from 1.2 to 2.0 μm at 1350 °C after annealing for 20 h. At the anode side, a temperature of 1400 °C was needed to initiate grain growth. The observed effect was attributed to supersaturated oxygen vacancies accumulated at the cathode side leading to reduction of the cations, which, in turn, lowers their migration barrier. When the pre-sintered material was only 70% dense before electric loading, grain growth was initially suppressed, while densification was enhanced by the presence of the electric current. Faster

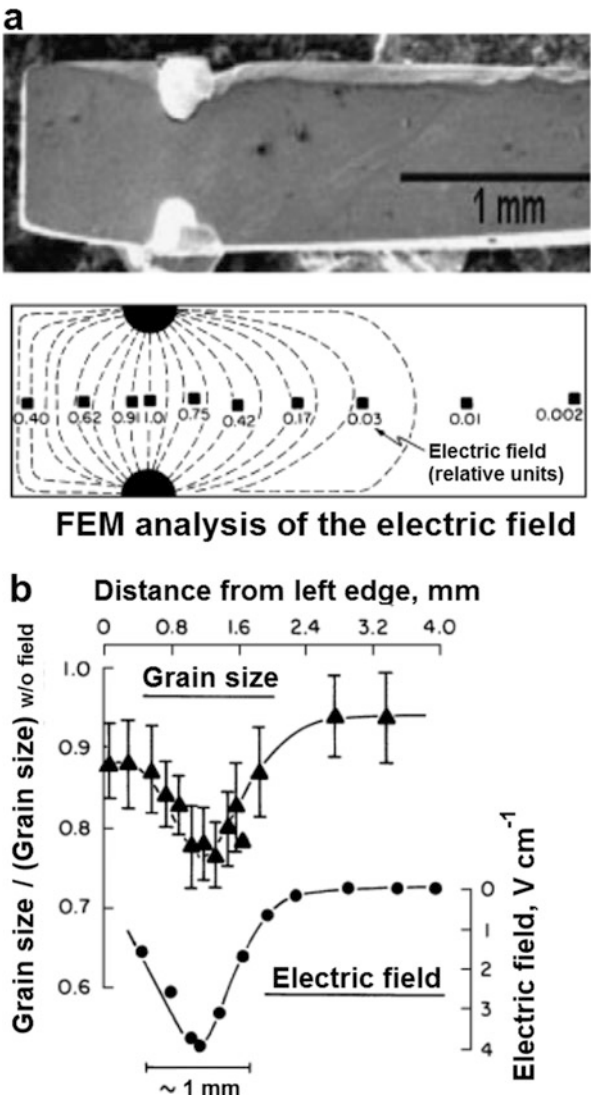

Fig. 1.14 The distribution of the electric field in the specimen obtained by finite element modeling (FEM) (**a**) and the spatial correspondence between the grain size and the magnitude of the applied field for 3 mol % yttria-stabilized zirconia (**b**). (Reprinted from Ghosh et al. [54], Copyright (2009) with permission of John Wiley & Sons)

densification occurred at the cathode side. After full densification was reached, the grain growth started at the cathode side.

Ghosh et al. [54] reported retarded grain growth under applied electric field for dense nanocrystalline 3 mol% yttria-stabilized zirconia prepared by the sinter-forging technique and annealed for 10 h at 1300 °C. The distribution of the electric field in the specimen obtained by the finite element analysis and the spatial correspondence between the grain size and the magnitude of the applied field are shown in Fig. 1.14a–b. The grain size in Fig. 1.14b is normalized with respect to the average grain size obtained without electric field. Among possible underlying mechanisms of

retarded grain growth, Ghosh et al. considered a thermodynamic effect of the minimum in the interfacial energy formed due to more intense Joule heating of the boundary having a higher electrical resistance than the grains.

Following the results reported by Ghosh et al., Holland et al. [55] performed a thermodynamic analysis of the grain growth suppression effect in the presence of a thermal gradient. They argued that in mixed or ionically conducting ceramics, no significant contribution of temperature gradients can be expected due to high thermal conductivities and nanometric grain sizes. Along this line, an explanation of the retarded grain growth in the presence of an electric field concerned with an altered grain-boundary mobility and enhanced solute segregation also suggested by Ghosh et al. [54] gains more importance.

The influence of the electric field on grain growth is especially important for nanograined materials, as the densification rate is inversely proportional to the fourth power of the gain size [56]:

$$\dot{\rho} = \frac{Af(\rho)}{Td^4} e^{-\frac{Q_b}{RT}}, \tag{1.5}$$

where A is the material constant, Q_b is the activation energy for self-diffusion at grain boundaries, $f(\rho)$ is a function of the density, T is the temperature, and d is the grain size. As is seen from the above expression, sintering accompanied by grain growth slows down significantly.

Another nonthermal effect of electric field is migration of pores and gas bubbles in ceramics. Such observations were reported by Kim et al. [57] for yttria-stabilized zirconia (8YSZ). Pores and gas bubbles migrated against the field at temperatures, at which the lattice and grain-boundary diffusion was frozen.

The significance of nonthermal effects is currently recognized in the area of microwave sintering. The first studies of the use of microwave radiation for high-temperature processing of materials date back to the 1960s [58]. In the field of microwave sintering of ceramics, the pioneering experimental work was done by Tinga and Voss [59], Berteaud and Badot [60], Meek et al. [61], and Johnson [62, 63]. It was found that microwave sintering has features of high importance for the industry, which include a significant (50–100 °C) decrease in the process temperature and a reduction in the duration of the high-temperature stage of the sintering process. One of the possible reasons for the latter is an inverse distribution of porosity at the intermediate stage of sintering due to volumetric heating, which facilitates densification [64]. The presence of nonthermal effects in microwave sintering was attributed to the action of ponderomotive forces, which reflect the influence of high-frequency electromagnetic fields on mass and charge transport in ionic crystalline solids [65–67]. The nature of ponderomotive forces is the interaction of the microwave field with the effective electric charges of vacancies. As the microwave-induced flux of vacancies oscillates at the microwave frequency, in order to exert influence on mass transport, it needs to be "rectified" through a certain mechanism that transforms the oscillatory motion into a monotonic drift. Such a mechanism has been elaborated by Rybakov et al. [65] and Olevsky et al. [66], who

suggested that rectification can be caused by perturbations of the vacancy flow near the pore surfaces of limited permeability for the vacancies.

The pinch effect is self-constriction of the sintered compact in the radial direction by the magnetic field of the current passing through the compact [22]. The distribution of the magnetic pressure over the sample's cross section is of a parabolic character and is more uniform when occurring simultaneously with the skin effect. The pinch effect helps eliminate the problem of friction between the compact and the die wall and maintain the porosity of the compacts as they are pressed out of the die (when the target material is a porous material).

The presence of surface oxides on metallic particles may slow the resistance sintering kinetics or accelerate it depending on the probability of their breakdown. If no breakdown occurs, the films act as barriers for electric current and hinder sintering kinetics. If breakdown of the films does take place, sparking between the particles can accelerate sintering.

Possible plasma effects still remain a controversial and open area of discussion within the field-assisted sintering scientific community. The formation of plasma requires certain levels of vacuum and voltage, which are different in various field-assisted sintering techniques. While high-voltage discharge compaction is routinely carried out in the presence of plasma-related phenomena, low-voltage modes of the field-assisted sintering (such as SPS) in most cases exclude these effects. Some localized plasma effects, depending on the processed material's chemical composition and structure characteristics, are claimed by some authors to be present during low-voltage-assisted processing too [68].

In the following book chapters, we describe in detail the underlying physical phenomena and the respective technical equipment for various known types of the field-assisted sintering techniques. We will demonstrate that the usually high rate of field-assisted processing is based on various transient thermal and nonthermal phenomena, which, if properly managed, provide a unique environment for densification and microstructure retention. In fact, in many cases, a successful field-assisted sintering process utilizes the conditions of *controlled non-equilibrium*.

References

1. Bordia R, Kang SJ, Olevsky EA (2017) Current understanding and future research directions at the onset of the next century of sintering science and technology. J Am Ceram Soc 100:2314–2335
2. Edison TA (1879) Electric Light. US Patent 219628
3. Voelker WL (1898) G.B. Patent 6149
4. Sauerwald F (1922) Apparatus for direct resistance heating to high temperature under pressure
5. Taylor GF (1933) Apparatus for making hard metal compositions. US Patent No. 1896854
6. Lenel FV (1955) Resistance sintering under pressure. JOM 7(1):158–167
7. Inoue K (1962) Electric Discharge sintering. US Patent 3241965
8. Inoue K (1966) Apparatus for electrically sintering discrete bodies. US Patent 3250892
9. Greenspan J (1976) Impulse resistance sintering of tungsten. Army Materials and Mechanics Research Center, USA

10. Tokita M (1993) Trends in advanced SPS spark plasma sintering systems and technology. J Soc Powder Technol Jpn 30(11):790−804
11. Omori M (2000) Basic research and industrial production using the spark plasma system (SPS). Mater Sci Eng A 287(2):183−188
12. Groza JR, Zavaliangos A (2000) Sintering activation by external electrical field. Mater Sci Eng A 287(2):171−177
13. Groza JR, Zavaliangos A (2003) Nanostructured bulk solids by field activated sintering. Rev Adv Mater Sci 5:24−33
14. Mamedov V (2002) Spark plasma sintering as advanced PM sintering method. Powder Metall 45(4):322−328
15. Munir ZA, Anselmi-Tamburini U, Ohyanagi M (2006) The effect of electric field and pressure on the synthesis and consolidation of materials: a review of the spark plasma sintering method. J Mater Sci 41(3):763−777
16. Munir ZA, Quach D, Ohyanagi M (2011) Electric current activation of sintering: a review of the pulsed electric current sintering process. J Am Ceram Soc 94(1):1−19
17. Orrù R, Licheri R, Locci AM, Cincotti A, Cao G (2009) Consolidation/synthesis of materials by electric current activated/assisted sintering. Mater Sci Eng R 63(4–6):127−287
18. Grasso S, Sakka Y, Maizza G (2009) Electric current activated/assisted sintering (ECAS): a review of patents 1906–2008. Sci Technol Adv Mater 10:1–24
19. Dudina DV, Mukherjee AK (2013) Reactive spark plasma sintering: successes and challenges of nanomaterial synthesis. J Nanomater 625218, 12 p
20. Dudina DV, Mukherjee AK (2013) Reactive spark plasma sintering for the production of nanostructured materials. In: Sinha S, Navani NK (eds) Nanotechnology series, vol. 4: nanomaterials and nanostructures. Studium Press LLC, USA, pp 237–264
21. Olevsky EA, Aleksandrova EV, Ilyina AM, Dudina DV, Novoselov AN, Pelve KY, Grigoryev EG (2013) Outside mainstream electronic databases: review of studies conducted in the USSR and post-soviet countries on electric current-assisted consolidation of powder materials. Materials 6:4375–4440
22. Yurlova MS, Demenyuk VD, Lebedeva LY, Dudina DV, Grigoryev EG, Olevsky EA (2014) Electric pulse consolidation: an alternative to spark plasma sintering. J Mater Sci 49:952–985
23. Raichenko AI (1987) Basics of electric current-assisted sintering. Metallurgiya, Moscow, p 128
24. Belyavin KE, Mazyuk VV, Min'ko DV, Sheleg VK (1997) Theory and practice of electric pulse sintering of porous materials. Minsk, Remiko, p 180 (in Russian)
25. Khasanov OL, Dvilis ES, Bikbaeva ZG (2008) Methods of compaction and consolidation of nanostructured materials and products. Textbook, Tomsk Polytechnic University Publishing, Tomsk, 212 p (in Russian)
26. Olevsky EA, Kandukuri S, Froyen L (2007) Consolidation enhancement in spark-plasma sintering: impact of high heating rates. J Appl Phys 102:114913
27. Crivelli IV, Esposito E, Mele G, Siniscalchi A (1973) Formatura per Spark Sintering. Metall Italiana 65(11):611–618
28. Zavodov NN, Kozlov AV, Luzganov SN, Polishchuk VP, Shurupov AV (1999) Sintering of metal powders by a series of heavy current pulses. High Temp 37(1):130–135
29. Zhou Y, Hirao K, Yamauchi Y, Kanzaki S (2003) Effects of heating rate and particle size on pulse electric current sintering of alumina. Scr Mater 48:1631–1636
30. Johnson DL (1990) Comment on "temperature-gradient-driven diffusion in rapid-rate sintering". J Am Ceram Soc 73(8):2576–2578
31. Chipman J (1926) The Soret effect. J Am Chem Soc 48:2577–2589
32. Shewmon P (1958) Thermal diffusion of vacancies in zinc. J Chem Phys 29(5):1032–1036
33. Schottky G (1965) A theory of thermal diffusion based on lattice dynamics of a linear chain. Phys Status Solidi 8(1):357–368
34. Kornyushin YV (1980) Influence of external magnetic and electric-fields on sintering, structure and properties. J Mater Sci 15(3):799–801

35. Searcy AW (1987) Theory for sintering in temperature-gradients-role of long-range mass-transport. J Am Ceram Soc 70(3):C61–C62
36. Young RM, McPherson R (1989) Temperature-gradient-driven diffusion in rapid-rate sintering. J Am Ceram Soc 72(6):1080–1081
37. Young RM, McPherson R (1990) Temperature-gradient-driven diffusion in rapid-rate sintering – reply. J Am Ceram Soc 73(8):2579–2580
38. Gostomelskiy VS, Krupnova LV (1985) Growth and healing of pores in metals under the action of current pulses. Phys Chem Mater Treat (Fizika I Khimiya obrabotki Materialov) 4:82–87 (in Russian)
39. Olevsky E, Froyen L (2009) Influence of thermal diffusion on spark-plasma sintering. J Am Ceram Soc 92:S122–S132
40. Chen W, Anselmi-Tamburini U, Garay JE, Groza JR, Munir ZA (2005) Fundamental investigations on the spark-plasma sintering/synthesis process I. Effect of dc pulsing on reactivity. Mater Sci Eng A 394(1–2):132–138
41. Kuz'mov AV, Olevskii EA, Aleksandrova EV (2013) Effect of micrononuniform heating of powder in field-assisted sintering on shrinkage kinetics. Powder Metall Met Ceram 51 (11–12):657–665
42. Mukherjee AK, Bird JE, Dorn JE (1969) Experimental correlation for high-temperature creep. Trans ASM 62:155–179
43. Tuchinskii LI (1982) Plastic relaxation of thermal stresses during sintering under nonisothermal conditions. Sov Powder Metall Met Ceram 21(11):849–853
44. Tuchinskii LI (1983) Possibility of plastic relaxation of thermal stresses in porous bodies. Sov Powder Metall Met Ceram 22(4):269–273
45. Skorokhod VV, Tuchinskii LI (1978) Condition of plasticity of porous bodies. Sov Powder Metall Met Ceram 17(11):880–883
46. Asoka-Kumar P, O'Brien K, Lynn KG, Simpson PJ, Rodbell KP (1996) Detection of current-induced vacancies in thin aluminum–copper lines using positrons. Appl Phys Lett 68:406
47. Garay JE, Glade SC, Anselmi-Tamburini U, Asoka-Kumar P, Munir ZA (2004) Electric current enhanced defect mobility in Ni_3Ti intermetallics. Appl Phys Lett 85:573
48. Frei JM, Anselmi-Tamburini U, Munir ZA (2007) Current effects on neck growth in the sintering of copper spheres to copper plates by the pulsed electric current method. J Appl Phys 101:114914
49. Burenkov GL, Raichenko AI, Suraeva AM (1987) Dynamics of interparticle reactions in spherical metal powders during electric sintering. Sov Powder Metall Met Ceram 26 (9):709–712
50. Olevsky E, Froyen L (2006) Constitutive modeling of spark-plasma sintering of conductive materials. Scr Mater 55:1175–1178
51. Cao WD, Lu XP, Sprecher AE, Conrad H (1990) Superplastic deformation behavior of 7475 aluminum alloy in an electric field. Mater Sci Eng A 129:157–166
52. Conrad H, Yang D (2010) Influence of an applied dc electric field on the plastic deformation kinetics of oxide ceramics. Philos Mag 90(9):1141–1157
53. Kim SW, Kim SG, Jung JI, Kang S-JL, Chen I-W (2011) Enhanced grain boundary mobility in yttria-stabilized cubic zirconia under an electric current. J Am Ceram Soc 94(12):4231–4238
54. Ghosh S, Chokshi AH, Lee P, Raj R (2009) A huge effect of weak dc electrical fields on grain growth in zirconia. J Am Ceram Soc 92(8):1856–1859
55. Holland TB, Anselmi-Tamburini U, Quach DV, Tran TB, Mukherjee AK (2012) Effects of local joule heating during the field assisted sintering of ionic ceramics. J Eur Ceram Soc 32 (14):3667–3674
56. Wang J, Raj R (1990) Estimate of the activation energies for boundary diffusion from rate-controlled sintering of pure alumina and alumina doped with zirconia or titania. J Am Ceram Soc 73:1172–1175
57. Kim SW, Kang SJL, Chen IW (2013) Ionomigration of pores and gas bubbles in yttria-stabilized cubic zirconia. J Am Ceram Soc 96(4):1090–1098

58. Osepchuk JM (1984) A history of microwave heating applications. IEEE Trans Microw Theory Tech 32(9):1200–1224
59. Tinga WR, Voss WAG (1968) Microwave power engineering. Academic Press, New York, p 1968
60. Berteaud AJ, Badot JC (1976) High temperature microwave heating in refractory materials. J Microw Power 11(4):315–320
61. Meek TT, Holcombe CE, Dykes N (1987) Microwave sintering of some oxide materials using sintering aids. J Mater Sci Lett 6(8):1060–1062
62. Johnson DL (1991) Microwave and plasma sintering of ceramics. Ceram Int 17:295–300
63. Johnson DL (1991) Microwave heating of grain boundaries in ceramics. J Am Ceram Soc 74 (4):849–850
64. Birnboim A, Gershon D, Calame J, Birman A, Carmel Y, Rodgers J, Levush B, Bykov Y, Eremeev A, Holoptsev V, Semenov V, Dadon D, Martin P, Rosen M, Hutcheon R (1998) Comparative study of microwave sintering of zinc oxide at 2.45, 30 and 83 GHz. J Am Ceram Soc 81:1493–1501
65. Rybakov KI, Olevsky EA, Semenov VE (2012) The microwave ponderomotive effect on ceramic sintering. Scr Mater 66:1049–1052
66. Olevsky EA, Maximenko AL, Grigoryev EG (2013) Ponderomotive effects during contact formation in microwave sintering. Model Simul Mater Sci Eng 21:055022
67. Rybakov KI, Olevsky EA, Krikun EV (2013) Microwave sintering: fundamentals and modeling. J Am Ceram Soc 96(4):1003–1020
68. Marder R, Estournès C, Chevallier G, Chaim R (2014) Spark and plasma in spark plasma sintering of rigid ceramic nanoparticles: a model system of YAG. J Eur Ceram Soc 35:211